Am J Cancer Res 2021;11(12):6147-6159
www.ajcr.us /ISSN:2156-6976/ajcr0139330

Original Article

Diacerein, an inhibitor of IL-1β downstream mediated apoptosis, improves radioimmunotherapy in a mouse model of Burkitt's lymphoma

Javeria Zaheer[1,3*], A Ram Yu[2*], Hyeongi Kim[1], Hyun Ji Kang[1,3], Min Kyoung Kang[2], Jae Jun Lee[2], Jin Su Kim[1,3]

[1]Division of RI Application, Korea Institute of Radiological and Medical Sciences, Seoul 01812, Republic of Korea; [2]Laboratory Animal Center, Osong Medical Innovation Foundation, Osong, Chungbuk 28160, Republic of Korea; [3]Radiological and Medico-Oncological Sciences, University of Science and Technology (UST), Seoul 01812, Republic of Korea. [*]Equal contributors.

Received September 23, 2021; Accepted October 31, 2021; Epub December 15, 2021; Published December 30, 2021

Abstract: Lymphoma has the characteristics of a solid tumor. Penetration of monoclonal antibodies is limited in solid tumors during radioimmunotherapy (RIT). Here, we first investigated the use of diacerein (DIA) as a combination drug to improve the penetration and therapeutic efficacy of ^{131}I-rituximab (RTX) using the Burkitt's lymphoma mouse model. We selected DIA through computational drug repurposing and focused on rheumatoid arthritis (RA) drug interaction genes to minimize side effects. Then, the cytotoxicity of DIA was assessed in vitro using three different lymphoma cell lines. DIA-induced apoptosis was confirmed by Western blotting. After confirming apoptosis, we confirmed the enhanced uptake of ^{131}I-RTX in Burkitt's lymphoma mouse model using SPECT/CT. Autoradiography of ^{131}I-RTX confirmed the therapeutic effect of DIA. Finally, the tumor size and survival rate were assessed to measure the enhanced therapeutic efficacy when DIA was used. In addition, we assessed the dose-dependency of DIA in terms of the accumulation of ^{131}I-RTX in tumor tissue, the tumor size, and the survival rate. The in vitro cytotoxicity was 10.9%. We showed that DIA induced apoptosis which was related to downstream IL-1β signaling by Western blotting. We found increased Annexin V positive apoptosis after DIA administration. Immuno SPECT/CT images demonstrated a higher uptake of ^{131}I-RTX in tumors in the DIA-administered group than that in the PBS-alone group. However, there were no statistical differences of dose-dependency between 20 mg/kg and 40 mg/kg of DIA. Tumor growth was significantly inhibited in the group treated with the combination of DIA plus ^{131}I-RTX at 7 days after injection. Our suggested combination of DIA and ^{131}I-RTX strategies could enhance the efficacy of ^{131}I-RTX treatment.

Keywords: Radioimmunotherapy, diacerein, ^{131}I, rituximab, drug repurposing, lymphoma

Introduction

Radiolabeled monoclonal antibodies (mAb) were considered as an effective modality for the treatment of relapsed and refractory Non-Hodgkin lymphoma (NHL) [1]. Rituximab (RTX) is a monoclonal antibody (mAb) for the CD20 antigen and kills lymphocytes by mAb-mediated cellular cytotoxicity [2, 3]. Radioimmunotherapy (RIT) uses radioisotope conjugated with mAb in the treatment of cancer [4]. RIT, using mAb labeled with radionuclides is an appealing procedure for cancer treatment because tumor linked-mAb with cytotoxic radionuclides can selectively bind to tumor antigen [4-6].

Most solid tumors have increased interstitial fluid pressure [7]. Increased tumor interstitial fluid pressure causes inefficient uptake of therapeutic agents [7]. For solid tumor RIT, high interstitial pressure was also the typical barrier to overcome [5]. Due to high interstitial pressure, mAbs cannot easily reach and uniformly be distributed to solid tumors, consequently reducing RIT efficacy [5]. To overcome limited penetration of mAb, co-administration of anticancer drugs was tried to decrease interstitial pressure and then induce apoptosis [5]. Their combination with RIT is an approach for the treatment of solid tumors wherein radioimmunotherapy alone has proven to be only reasonably ineffective [5, 8].

Lymphoma is a solid tumor by definition from the National Cancer Institute (https://www.cancer.gov/publications/dictionaries). The characteristics of the extracellular matrix in lymphoma cells represent those of solid tumors [9]. In a previous study, we showed that atorvastatin induces apoptosis and enhances the therapeutic efficacy of ^{131}Iodine (^{131}I)-RTX [10].

Diacerein (DIA), an interleukin (IL)-1β inhibitor, belongs to the anti-inflammatory class and was approved by the Food and Drug Administration for the treatment of osteoarthritis [11]. DIA protects against glycerol-induced acute kidney injury through the amelioration of AKI via its antioxidant, anti-inflammatory, and antiapoptotic effects [12]. DIA has some therapeutic applications. It diminishes IL-1-induced skin inflammation in psoriasis and attenuates IL-1-induced development of atherosclerosis [13].

However, in our study, we showed that DIA induced apoptosis in Burkitt's lymphoma cell lines. Micro-distribution of mAb inside tumors was assessed at the cellular level by quantifying its penetration using high-resolution fluorescence imaging. Therefore, we investigated whether DIA enhances the therapeutic efficacy of ^{131}I-RTX using a mouse model of Burkitt's lymphoma. Conversely and to the best of our knowledge, there is a paucity of reports using DIA as a combinational drug for RIT response enhancement.

Materials and methods

Computational drug repurposing

The Raji cell line (CLS Cat# 300359) expressions of genes were obtained from EMBL RNA cell line gene expression database with cutoff point 0.5 TPM (http://www.ebi.ac.uk/gxa/experiments/E-MTAB-2770/Results). Rheumatoid arthritis (RA) drug-interacting genes were from the Comparative Toxicogenomics Database (CTD) (http://ctdbase.org/) [14] and web-based free software FunRich (http://www.funrich.org/) using the Venn tool [15]. Side effects were evaluated by prediction count based on the L1000 database (http://maayanlab.net/SEP-L11000/index.html) [16]. We predicted drug profile-based similarity with Raji cell line and side effect-based comparison and selection. The steps involved in this process are as follows: Step 1. Data set A. Genes for the Raji cell line were downloaded from the EMBL database at the cut-off point was 0.5 TPM. Step 2. Chemical interacting genes for RA drugs were obtained from the CTD database, corresponding to data set B. Step 3. Each drug-interacting gene was overlapped with the Raji cell expression gene. Step 4. Jaccard Index (JI) was calculated as data set A interacting with data set B over data set A union with data set B minus data set A interacting dataset B. Mathematical equation is described as follow:

$$JI = \frac{(A \cap B)}{(A \cup B) - (A \cap B)}$$

Cell viability

Raji cells were maintained in Roswell Park Memorial Institute (RPMI) media containing 5% antibiotics and supplemented with 10% fetal bovine serum (FBS) (Sigma, St. Louis, MO, USA) at room temperature of 37°C in a humidified 5% CO_2 incubator. Cells were cultured in 96-well microtiter plates at initial densities of 1×10^5 cells/mL per well. The monolayer of cells in the plate was exposed to different concentrations of DIA (10, 20, 30, and 40 μM/well). After 48 h of culture, 100 μL of alamarBlue reagent (Invitrogen, Thermo Fisher Scientific) was added for 30 min to 1 h, and the absorption of the samples was measured using a fluorescent spectrophotometer with endpoint measurement (excitation at 560 nm and emission at 590 nm). The number of viable cells becomes highly fluorescent and turns pink in color, which is directly proportional to the number of metabolically living cells in the well.

Further, we investigated the potential effect of combinational therapeutic effect of DIA on lung cancer cell lines (e.g., NCI-H460, NCI-H1299, and A549), and breast cancer cell lines (e.g., JIMT-1).

Western blotting

In vitro, Raji cell lines were treated for 48 h with DIA (40 μM) and DMSO. Protein extracts were generated from the extraction buffer (Abcam, UK). Lysates were measured for protein concentration using the BSA assay kit (Thermo Fisher Scientific, USA), and proteins were further separated by Tris-glycine gel electrophoresis and transferred to nitrocellulose membranes using blot 2 Dry Blotting System

(Thermo Fisher Scientific, USA). The membranes were blocked with Tris-buffered saline (TBS) containing 5% non-body fat dried milk and 0.05% of Tween 20 (TBST) and incubated with the required antibodies. Primary antibodies used are Cytochrome C antibody (ab13575, Abcam, UK) at 1:1000 dilution (5% skim milk), Bcl-2 antibody (ab59348, Abcam, UK) at 1:500 dilution (5% skim milk), Bcl-xL antibody (ab32370, Abcam, UK) at 1:1000 dilution (5% skim milk), Caspase 3 antibody (ab32351, Abcam, UK) at 1:5000 dilution, Bax antibody (ab 32503, Abcam, UK) at 1:1000 dilution (5% skim milk) and β-Actin (ab6276, Abcam, UK) at a 1:5000 dilution (5% skim milk). Overnight incubation with primary antibody was followed by respective incubation with secondary antibodies at 1:5000 dilution (5% skim milk) for 1 h. at room temperature. Immunoreactive protein bands were visualized via enhanced chemiluminescence (ECL) reaction (Thermo Fisher Scientific USA). Images were captured with Amersham™ Imager 600 (GE Healthcare Life Sciences, USA) and scanned.

Animal care

All animals experiments were performed according to the Institutional Animal Care and Use Committee (IACUC) protocol (IACUC no.: KBIO-IACUC-2020-014, KIRAMS 2018-0016) of the Osong Medical Innovation Foundation (K-BIO) and Korea Institute of Radiological and Medical Sciences (KIRAMS), respectively.

The study was approved and reported following ARRIVE guidelines.

Lymphoma xenograft subcutaneous model

Five-week-old female NOD.CB17/SCID mice (Koatech, Korea) were maintained in temperature-controlled clean racks with a 12-h light/dark cycle and allowed to acclimatize for 1 week before the start of the experiment. Approximately 5×10^6 Raji cell lines were injected subcutaneously in the right flank. When the tumor size reached approximately 200 mm^3, mice were randomized into each group (n=7/group). Each group was treated with a single dose of PBS, ^{131}I-RTX (150 μg, 12.95 MBq), ^{131}I-RTX (150 μg, 12.95 MBq) plus DIA (20 mg/kg), and ^{131}I-RTX (150 μg, 12.95 MBq) plus DIA (40 mg/kg). The tumor size was measured at indicated times using a digital caliper, and the formula (width/2 × length/2 × depth/2) was applied to calculate the tumor volume. The mouse survival rate was measured.

Penetration and distribution studies

Grouping based on penetration and distribution studies consisted of 3 groups with 5 mice each. Each group received 150 μg RTX conjugated to Alexa 647 with or without DIA, which was intraperitoneally administered at 20 mg/kg or 40 mg/kg for 5 days.

Preparation of Alexa647-rituximab

A solution of Alexa Fluor 647 NHS Ester (1 mg, Invitrogen, USA) dissolved in 155 μl dimethyl sulfoxide (DMSO) containing 1% acetic acid was immediately mixed with 500 μl of RTX (Genetech, CA, USA) and 250 μl of 1 M sodium bicarbonate solution, pH 8.5. The solution was incubated for 1 h at room temperature. Alexa 647-RTX was purified using a size-exclusion PD-10 column (GE Healthcare Bio-Sciences AB, Sweden) and eluted with phosphate-buffered saline (PBS). The level of Alexa 647 molecules conjugated per RTX was estimated using the Alexa 647 peak intensity distributed between the mAb-Alexa 647 conjugate and free Alexa-647 eluted from the size-exclusion HPLC.

Rituximab penetration studies

Upon reaching the tumor size 200±20 mm^3, Alexa 647-RTX (150 μg in 100 μl of PBS) was intraperitoneally administered to Raji-bearing mice, and DIA (20 mg/kg or 40 mg/kg) was injected for 5 days. At 5 days after injection of Alexa 647-RTX, the mice were euthanized via CO_2 inhalation and exsanguinated via cardiac puncture before dissection.

Immunofluorescence staining

Tumors were isolated and fixed with 4% paraformaldehyde overnight at 4°C. Tumors were embedded with 30% sucrose in a PBS solution until the tissue sank to the bottom of the tube at 4°C and was frozen in an OCT compound (Sakura Finetec, USA). Frozen tumors were sectioned with 8 μm thickness using a cryostat microtome (CM1800; LEICA Instruments) in three different cross-sectional areas (25%, 50%, and 75% from the tumor apex) throughout the tumors. Next, 7 sections were randomly

selected from each cross-sectional area from 4 different tumors. Tumor sections, fixed for 10 minutes in 4% paraformaldehyde, were washed with PBS for 5 minutes three times and mounted with Prolong Gold antifade reagent with 4, 6-diamidino-2-phenyindole (DAPI) (Invitrogen, USA).

Acquisition and analysis of fluorescent images

The fluorescent images were acquired with a 10× objective using an In cell analyzer (GE Healthcare, Uppsala, Sweden). DAPI for nuclei (shown in blue, Ex/Em =358/461 nm), FITC for Alexa 647-Annexin V (shown in orange, Ex/Em =488/525 nm), and Cy5 for Alexa 647-RTX (shown in green, Ex/Em =594/633 nm) were obtained.

Image analysis was performed using MATLAB (Math Works, Natick, MA, USA) and MIPAV (National Institutes of Health, Bethesda, MD, USA), two program software written in-house. Briefly, TIFF files were exported and read by plotting a line graph using MIPAV software. RTX intensity from the tumor edge was calculated by drawing the volume of interest (VOI) line perpendicular from the edge towards the center. The RTX signal intensity was measured in correspondence to a 30 μm line distance. The resulting graph depicting line intensity vs line distance was read using MATLAB. The AUC analysis (three tumors with 10 sections in each tumor (n=30) in each group) was used to evaluate the penetration of RTX from the tumor edge. Total accumulation was calculated by drawing the region of interest (ROI) across the whole tumor (not included any skin, muscle, capsular tissue attached). The area under the curve (AUC) was calculated. The whole tumor area was calculated using free-drawn ROI using MIPAV. The total Alexa 647-RTX intensity was then normalized by the whole tumor area.

To quantify the number of annexin V-positive cells in terms of the fraction of apoptosis across the tumor tissue in the slide, the fuzzy C-means clustering method (number of classes: 3, desired exponent value: 2, end tolerance: 0.01, the maximum number of iterations: 200) was performed. The apoptotic region fraction was calculated from a binary image that was acquired with the fuzzy C-means clustering method [17].

^{131}I-radiolabeling with RTX

^{131}I-radiolabeling with RTX was conducted as described previously [18]. After labeling, instant thin-layer chromatography (solvent, 100% C_3H_6O) showed that the radiochemical purity of ^{131}I-RTX was >95%. The immunoreactivity of ^{131}I-RTX was 95.0%, as defined using a cell-binding assay, and the specific activity was 0.32 mCi/mg (Supplementary Figure 1).

Immuno-SPECT images of ^{131}I-RTX

All SPECT scans in this study were performed using a nano SPECT/CT scanner (Mediso, Hungary). When the tumor size reached approximately 200 mm^3 at 3-4 weeks after tumor implantation, ^{131}I-RTX (150 μg, 16.2-19.3 MBq/200 μL) was intravenously injected into the NOD.CB17/SCID mouse. The mice were randomly divided into two groups (n=7 per group). DIA (40 mg/kg) was intraperitoneally administered daily for 5 days, and PBS was administered in the control group. Six days after ^{131}I-RTX injection, the mice were anesthetized with 2.0% isoflurane, and SPECT data were obtained using a four-headed multiplexing multi-pinhole collimator. Each head was fitted with an application-specific tungsten collimator with 16 pinholes. We used a mouse aperture (M^3 high-energy mouse whole-body aperture), which comprises a total of 64 individual 1.7-mm diameter pinholes. The axial FOV is extended using a step-and-shoot helical scan, defining a range of mouse whole body. The energy peak for the camera was set at 364.5 keV, and the energy window was 328-400 keV. An acquisition time of 50 s per view was selected, resulting in acquisition times ranging from 50 to 60 min per animal. Reconstruction of the images was performed with attenuation correction, the matrix size was 128 × 128 × 360, and voxel size was 0.234 × 0.234 × 0.234 mm^3. In the acquisition of the anatomical image, CT in mice was performed with 50 kVp, 720 μA, and 300 ms exposure time. The effective pixel size of the reassembled CT image was 229.28 μm × 229.28 μm. Visualization and quantification of images were performed using the InterView FUSION software (ver 3.0). Immuno-SPECT images of ^{131}I-RTX were performed at acquired at a subsequent time interval at 1 h, 1 day, 2 days, 3 days, and 4 days. The activity data were presented as the percentage of injected radioactivity dose

per gram of tissue (%ID/g). SPECT and CT images were co-registered using InterView FUSION software (ver 3.0). After co-registration of CT and SPECT data, the ROI was sketched on the CT image and photocopied to the SPECT data. %ID/g was calculated by

$$\%ID/g = C_T \times CCF \times \frac{V_T}{W_T} \times \frac{1}{D_{inj} \times 2^{\frac{t}{\lambda}}} \times 100\%$$

Where C_T is radioactivity of maximal counts per voxel in ROI (Counts/second/voxel); D_{inj} is the injected dose (mCi); W_T is weight in the tissue region (g); V_T represents volume (cc); CCF is calibration factor (voxel × uCi/cc/cps); λ is Half-life of Cu-64 (min); t is time point (min); The tissue density was assumed to be approximately 1 cc/g of tissue. C_T value was obtained from a SPECT ROI, and CCF was calculated using a cylinder calibration factor. The quantification of ^{131}I-RTX accumulation in tumors was represented by %ID/g (*P<0.05, **P<0.005). %ID/g for individual images were calculated on the SPECT images and %ID/g is evaluated for each time point for up to 4 days. The ROI was drawn along the tumor margin using the free drawing option. ROI size was 25 mm^2.

Autoradiography

Immediately after CT/SPET scanning, tumor tissues were isolated and frozen in an OCT compound. 48 h later, frozen tumors were sectioned with 20 μm thickness using a cryostat microtome and exposed on an imaging plate for 24 h. The plates were scanned with BAS-5000 (Fujifilm, Tokyo, Japan). Multi Gauge software (version 3.0; Fujifilm) was used to quantify the intensities of tumor uptake of ^{131}I-RTX or ^{131}I-RTX plus DIA as units of photostimulated luminescence per square millimeter (PSL/mm^2).

Radioimmunotherapy

When the tumor volume was approximately 200 mm^3 in Raji-bearing mice, mice were randomized into 3 groups (n=7 per group) and treated with a single dose of PBS, ^{131}I-RTX (150 μg, 12.95 MBq), or ^{131}I-RTX (150 μg, 12.95 MBq) plus DIA (20 mg/kg or 40 mg/kg), respectively. The tumor size was measured by using a digital caliper, and the tumor volume was calculated three times a week from the following formula: width^2 × length × 0.4.

Statistical analysis

Data are expressed as mean ± SD and were found to be normally distributed. A two-tailed student's t-test was used. * denoted P<0.05, ** denoted P<0.005, *** denoted P<0.0005. All statistical analyses were performed using PRISM statistical software (ver 5.0, Graphpad software; San Diego, CA, USA), and all P-values of <0.05 were considered statistically significant.

Results

DIA selection based on computational drug

Figure 1 shows drugs with the potential of similarity to the Raji cell lines by considering the Jaccard Index. DIA scored low; however, DIA overlapped 5 of 9 DIA interacting genes with the Raji cell lines with only 16 side effect count. The count was conducted via side effect prediction based on the L1000 database. Therefore, we combined DIA with ^{131}I-RTX to enhance the therapeutic efficacy of combination RIT. DIA was selected as a putative cytotoxic drug based on drug-based knowledge. DIA was overlapped with 5 out of 4 DIA interacting genes including Bax with 17831. Raji cell line expressed genes thus scoring a Jaccard index of 0.02. The gene interaction of each rheumatoid arthritis (RA) drug and their Jaccard Index (JI) is presented in **Figure 1A**. Then, we obtained the side effect count by checking listed predicted side effects for each drug based on the L1000 database. DIA only had a 16 side effect count, thus scoring the lowest. Therefore, we selected DIA for its gene interaction with the Raji cell lines and low side effect count. **Figure 1B** shows the side effect prediction count of RA drugs. **Figure 1C** shows the structure of DIA.

Apoptotic effect of DIA

The cell viability of Raji cells was dose-dependently decreased by DIA (**Figure 2A**). The western blotting result shows DIA-induced apoptosis (**Figure 2B** and Supplementary Figure 4). DIA also induced cytotoxicity to lung cancer cell lines such as A549, NCI-H460, NCI-H1299, and breast cancer cell lines such as JIMT-1 (Supplementary Figure 2). We selected the Raji cell xenografted mouse model to show the potential drug for combinational therapy with ^{131}I RTX. The therapeutic efficacy of DIA was tested with Raji cell line xenograft and tumor

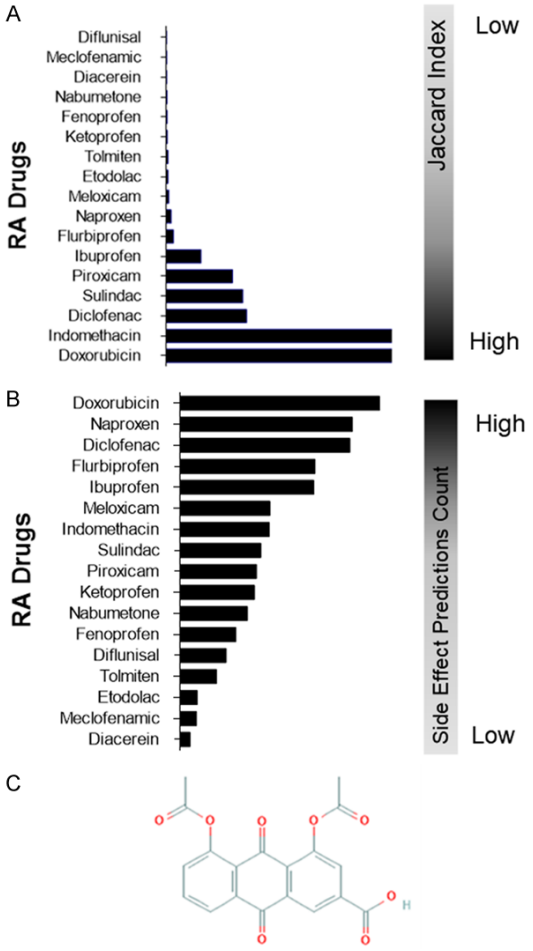

Figure 1. DIA was selected as a putative cytotoxic agent based on computational drug-based knowledge. A. DIA shows a Jaccard Index of 0.02 when tested for interacting gene in rheumatoid arthritis (RA) drugs intersected with Raji cell line expressed genes. B. The selected drugs were filtered for the least side effect prediction count. DIA scored the lowest, with a side effect count of 16. Doxorubicin is used as a standard for cytotoxic drugs. C. Structure of DIA exported from PubChem.

volume, and a survival study was performed. At 23 days, tumor volumes of DIA treated groups were significantly smaller than that of the PBS group (2851.6±1199 mm^3 for PBS group *vs* 1173±110 mm^3, ***P<0.0005). The efficacy of the xenografts treated with DIA increased at a slower rate than that of PBS treatment. The survival rates in the DIA group were also significantly greater compared with those in the PBS group alone (**Figure 2C**, **2D**).

Diacerein improves rituximab penetration across tumor

We evaluated the micro-distribution of RTX across Raji lymphoma tumor tissues with DIA. We investigated whether the addition of DIA could increase RTX penetration inside tumor tissues. To evaluate the effect of DIA, we injected Alexa 647-RTX (150 µg/100 µl, n=7) with 20 mg/kg or 40 mg/kg DIA (n=7). **Figure 3A** shows the representative images of Alexa 647-RTX in combination with DIA. The fluorescent intensity of RTX extravasated from the tumor edge and across the whole tumor was quantified in both groups. We found increased Annexin V positive apoptosis after DIA administration (**Figure 3B**). The average fraction of apoptotic region was 11% (for control), 12% (for 20 mg/kg of DIA), 18% (for 40 mg/kg of DIA), respectively. We then observed that the RTX in combination with DIA improved the Alexa 647 conjugated RTX across the whole tumor section (n=20), as shown in **Figure 3C**. The area under the curve (AUC) from the tumor edge 1921 for Alexa 647-RTX, where it was improved to 3748 or 5248 in case of combination treatment with 20 mg/kg or 40 mg/kg of DIA (**Figure 3D**).

Immuno SPECT images of ^{131}I-RTX with DIA

ImmunoSPECT/CT images were obtained at 1 h, 1 day, 2 days, 3 days, and 4 days after injection of ^{131}I-RTX. As shown in **Figure 4**, immunoSPECT/CT images demonstrated a higher uptake of ^{131}I-RTX in tumors in the DIA-administered group than that in the PBS-alone group. We found that there was a significant increase of %ID/g for ^{131}I-RTX plus DIA compared to ^{131}I-RTX alone (*P<0.05, shown in **Figure 4B**). The tumor uptake was 5.91±3.2 in the ^{131}I-RTX-alone group, 16.1±1.9 in the ^{131}I-RTX + 20 mg/kg of DIA, and 18.2±1.0 in the ^{131}I-RTX + 40 mg/kg of DIA group 4 days after injection of ^{131}I-RTX (**Figure 4B**). Combination RIT of ^{131}I-RTX with DIA shows improved %ID/g where the time point 1 day, 2 days, 3 days, and 4 days are statistically significant (***P<0.005*). However, there were no statistical differences of dose-dependency between 20 mg/kg and 40 mg/kg of DIA. Autoradiography showed a 3.2-fold and 4.7-fold greater tumor uptake of ^{131}I-RTX in 20 mg/kg and 40 mg/kg of DIA plus ^{131}I-RTX-treated group than ^{131}I-RTX-treated group, respectively (**Figure 4C**, ***P<0.0005). **Figure 4D** shows the tumor volume as time passes for 7 days in Raji-xenograft models. We observed aggressive progression of the tumor occurred in the mice treated with PBS alone. Tumor growth was significantly inhibited in the group treated with the combination of 40 mg/kg of DIA plus ^{131}I-RTX, with a volume of

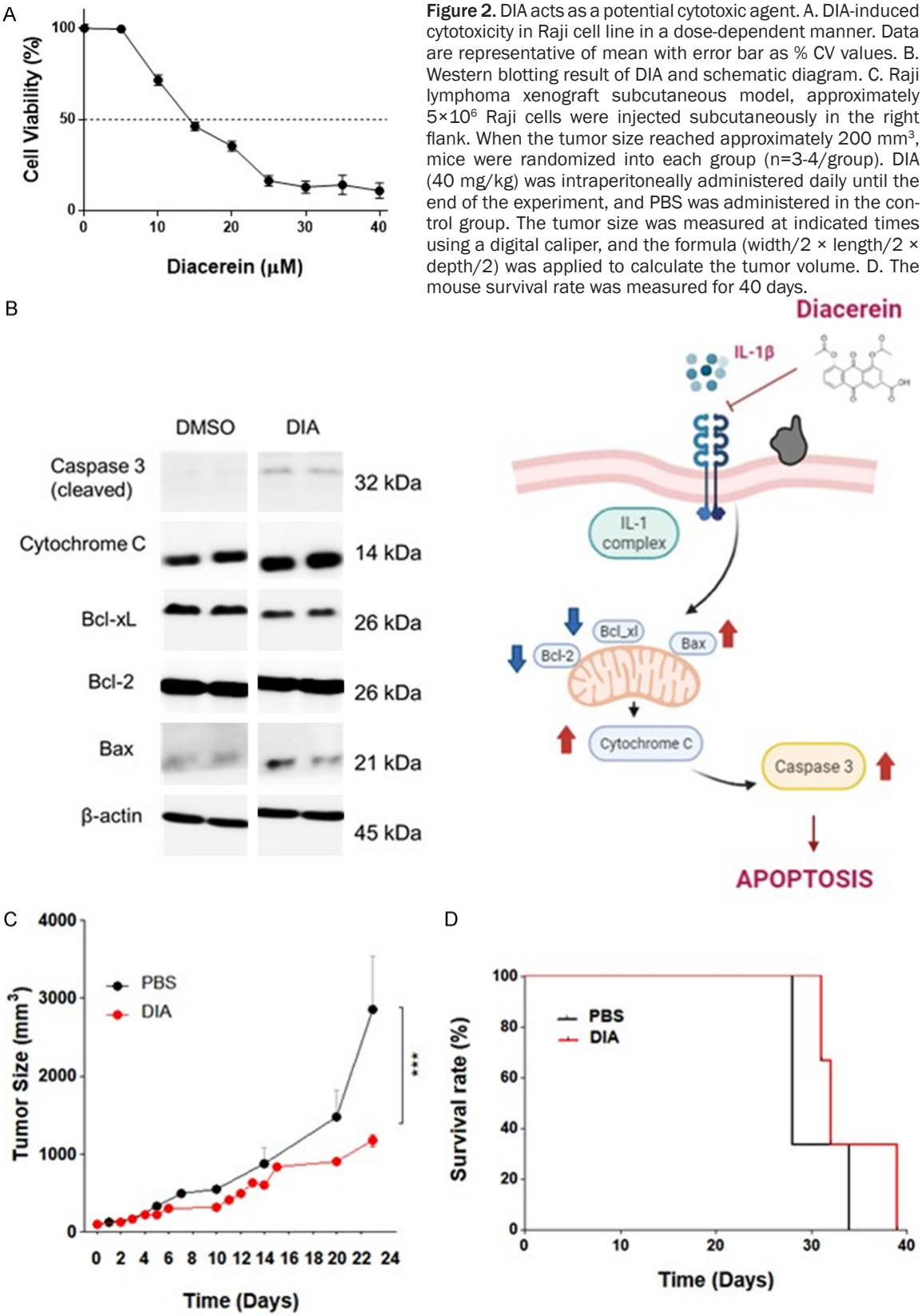

Figure 2. DIA acts as a potential cytotoxic agent. A. DIA-induced cytotoxicity in Raji cell line in a dose-dependent manner. Data are representative of mean with error bar as % CV values. B. Western blotting result of DIA and schematic diagram. C. Raji lymphoma xenograft subcutaneous model, approximately 5×10^6 Raji cells were injected subcutaneously in the right flank. When the tumor size reached approximately 200 mm^3, mice were randomized into each group (n=3-4/group). DIA (40 mg/kg) was intraperitoneally administered daily until the end of the experiment, and PBS was administered in the control group. The tumor size was measured at indicated times using a digital caliper, and the formula (width/2 × length/2 × depth/2) was applied to calculate the tumor volume. D. The mouse survival rate was measured for 40 days.

195.9±46.3 mm^3 than PBS group (534.1±81.4 mm^3) at 7 days after injection (***P<0.0005). The tumor volume with the combination of 20 mg/kg of DIA plus ^{131}I-RTX was 215.9±33.8

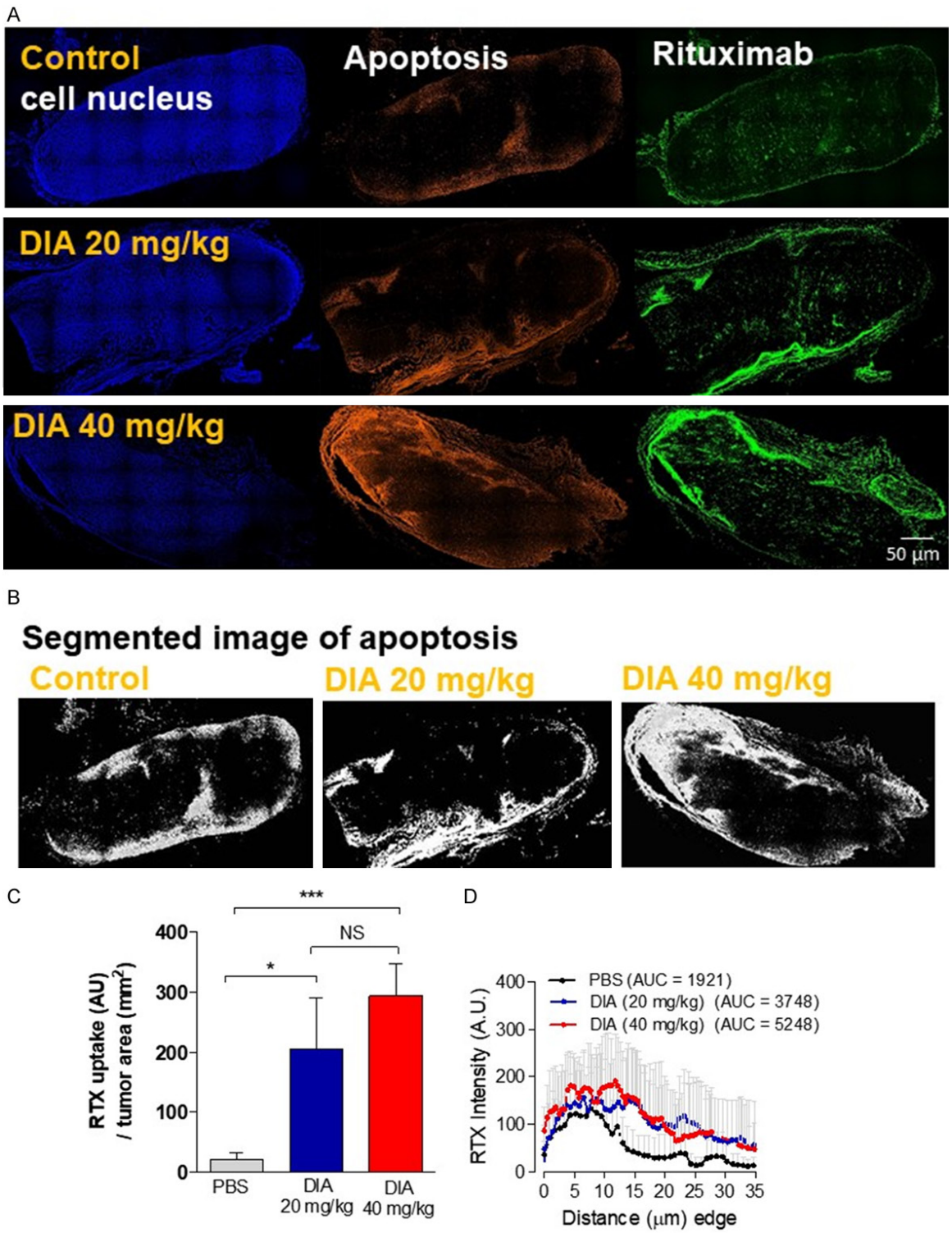

Figure 3. Rituximab penetration studies. A. Upon reaching the tumor size 200±20 mm^3, Alexa 647-RTX (150 μg in 100 μl of PBS) was intravenously injected into Raji-bearing mice, and diacerein (40 mg/kg) was intraperitoneally administered for 5 days. The fluorescent images were acquired with a 10× objective using an In cell analyzer (GE Healthcare, Uppsala, Sweden). DAPI for nuclei (shown in blue, Ex/Em =358/461 nm), FITC for Alexa 647-Annexin V (shown in orange, Ex/Em =488/525 nm), and Cy5 for Alexa 647-RTX (shown in green, Ex/Em =594/633 nm) were obtained. B. Segmented image of apoptosis using fuzzy C-means clustering method. C. The total Alexa 647-RTX accumulation was normalized by total tumor area: Total tumor intensity of mAb = intensity of mAb in the tumor/total tumor area. Here, the total tumor area was measured using free-drawn ROI using MIPAV. D. RTX intensity from the

edge of the tumor was calculated by drawing the volume of interest (VOI) line perpendicular from the edge towards the center. The resulting graph depicting line intensity vs line distance was read in MATLAB. The RTX signal intensity was measured in correspondence to a 30 μm line distance. The AUC analysis from three tumors with 10 sections in each tumor (n=30) and in each group was used to calculate the penetration of RTX from the tumor edge. Scale bar indicates 50 μm.

mm^3. Within 7 days, tumor size was reduced to less than the size of the tumor at the starting point when DIA plus ^{131}I-RTX was used.

Discussion

In this study, we first showed that DIA could be used as a combinational drug to improve the therapeutic effect of ^{131}I-RTX. **Figure 1** shows that DIA is one of the RA drugs that has the least adverse effects as confirmed by computational drug repurposing. *In vitro* and *in vivo* studies, as well as Annexin V apoptosis assay were performed to confirm the cytotoxicity and therapeutic effects of DIA (**Figures 2** and **3**). When DIA was intraperitoneally administered to mice, the tumor size was dramatically reduced (**Figure 2**), and enhanced accumulation of RTX or ^{131}I-RTX uptake was observed (**Figures 3** and **4**).

The enhanced uptake of RTX and increased therapeutic effect of ^{131}I-RTX can be explained by apoptosis within the tumor tissue. Induced apoptosis possibly induces decreased interstitial pressure within tumor tissue. We confirmed that there is a downstream pathway that induces apoptotic and cytotoxic DIA effects for lymphoma cell lines such as Raji cell lines (shown in **Figure 2A**, **2B**). The principal mechanism of action for DIA is to inhibit the IL-1β system and related downstream signaling [19]. Western blotting indicated that apoptosis was induced by IL-1β related downstream signaling when DIA was applied. The protein levels of Caspase 3, Cytochrome C, and Bax increased. In addition, the protein levels of Bcl-2 and Bcl-xl decreased (shown in **Figure 2B** and Supplementary Figure 4).

DIA is originally a non-steroidal anti-inflammatory drug to treat symptomatic slow-acting osteoarthritis [11]. DIA is used clinically for anti-inflammatory and anabolic properties [11]. At a daily oral dose of 50 mg/kg, DIA is known to carry out efficacious anti-inflammatory and analgesic actions and may even have slight disease-modifying actions in patients with osteoarthritis [20], beneficial in improving joint pain in humans and rodent models [21] and have shown to reduce the incidence of diabetes [22, 23]. Recent studies have explored the roles of pharmacological activities of DIA, including anti-testicular injury and anti-cervical hyperkeratosis effects via anti-inflammatory, antioxidant, and anti-apoptotic activities [24]. DIA was found to protect against cadmium-induced testicular toxicity at a dose of 50 mg/kg/day [25]. Recent studies have shown that DIA has protective effects against subchondral bone remodeling, and the recommended starting dose is 50 mg once daily with the evening meal for the first 2-4 weeks of treatment [26].

Herein, we showed the anti-cancer effect of DIA. Recent emerging evidence suggests that DIA has significant antitumor effects, supporting the potential use of DIA as an antitumor agent [27]. Inflammatory cytokines like IL-6 have been reported in the development and progression of not only in many inflammatory conditions but also in cancer [28]. An increased level of IL-6 has been reported in a wide range of cancers, such as breast cancer [29]. DIA regulated inhibition of breast cancer via IL-6 modulation. DIA-prompted apoptosis has been correlated with the suppression of IL-6/STAT3 [30, 31].

Combination RIT is a pragmatic approach whereby the drug's adjunction or other agents not only facilitate mAbs to reach the targeted site but also enhance its effectiveness [6]. Although NHL is a hematological tumor, the characteristic of NHL is solid tumor-like [9, 10]. Thus, the combination of drugs or moieties with RIT can be applied to overcome the barriers that RIT alone faces for solid tumors [5, 32]. High-intensity focused ultrasound reduced interstitial pressure, then increased the penetration of the mAb [33]. We demonstrated that penetration and uptake of trastuzumab or anti-PD1 were also enhanced after inducing apoptosis when combination gene therapy was applied [34]. The recent advent of α-particle RITs is a promising potential therapeutic agent used in oncology [35-42]. When α-particles such as

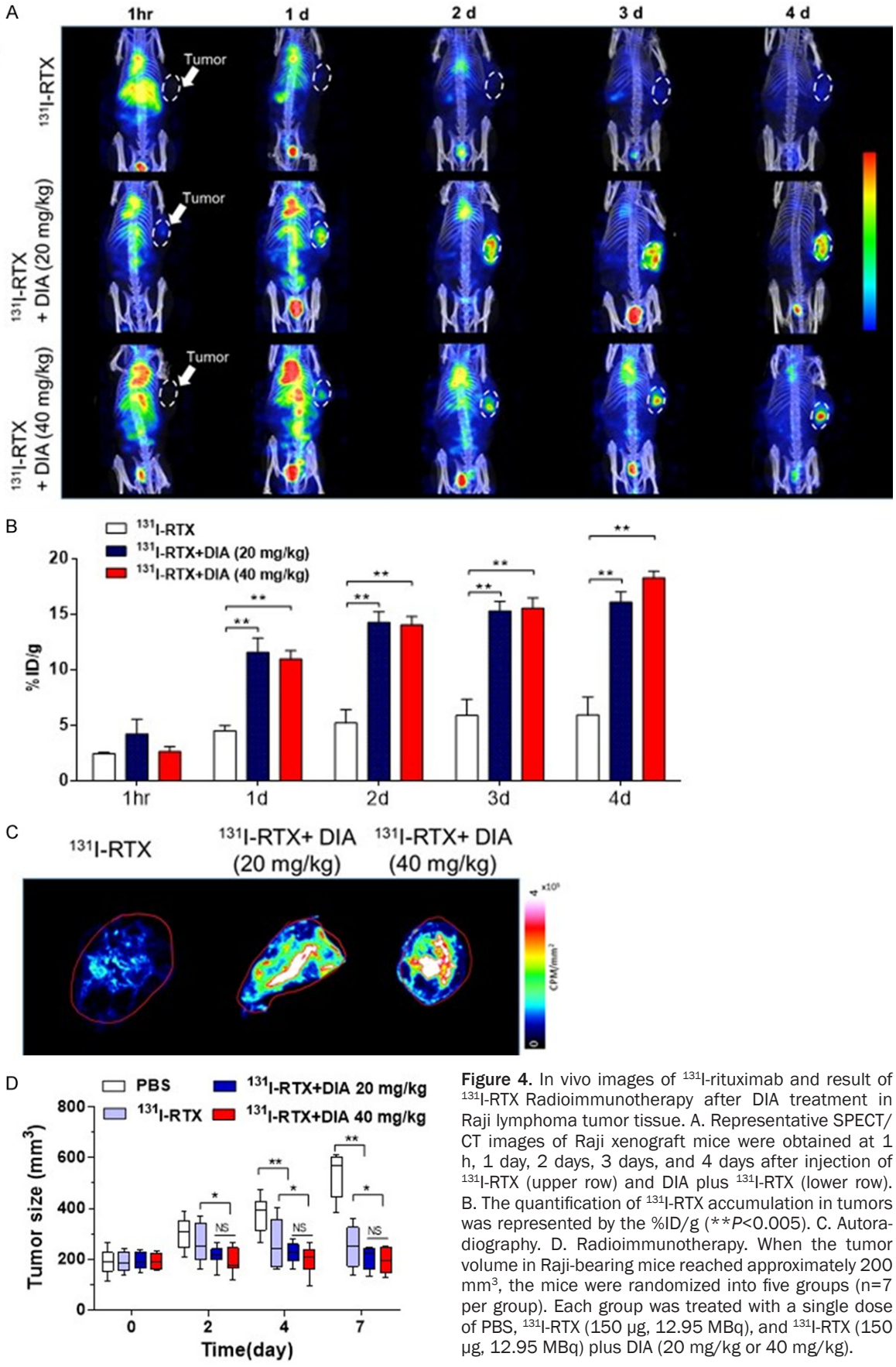

Figure 4. In vivo images of ^{131}I-rituximab and result of ^{131}I-RTX Radioimmunotherapy after DIA treatment in Raji lymphoma tumor tissue. A. Representative SPECT/CT images of Raji xenograft mice were obtained at 1 h, 1 day, 2 days, 3 days, and 4 days after injection of ^{131}I-RTX (upper row) and DIA plus ^{131}I-RTX (lower row). B. The quantification of ^{131}I-RTX accumulation in tumors was represented by the %ID/g (***P*<0.005). C. Autoradiography. D. Radioimmunotherapy. When the tumor volume in Raji-bearing mice reached approximately 200 mm^3, the mice were randomized into five groups (n=7 per group). Each group was treated with a single dose of PBS, ^{131}I-RTX (150 μg, 12.95 MBq), and ^{131}I-RTX (150 μg, 12.95 MBq) plus DIA (20 mg/kg or 40 mg/kg).

^{211}At ($t_{1/2}$, 7.2 h), ^{213}Bi ($t_{1/2}$, 46 min), ^{225}Ac ($t_{1/2}$, 10 days), and ^{233}Ra ($t_{1/2}$, 11 days) are used for RIT [38, 43-45], deeper penetration and uniform accumulation is of paramount importance because its range was <50 μm [5]. Therefore, our suggested combinational strategies would be helpful for α-particles RIT.

In general, 50 mg/kg of DIA was also used in mouse or rat studies. 50 mg/kg IP of DIA protected doxorubicin-induced nephrotoxicity in a rat study [46] and was used to decrease visceral pain in mice [21]. In humans, 50 mg and 100 mg of DIA once a day or twice a day is a recommended dose [26]. 150 mg of DIA twice a day (max 300 mg) is also administered in humans with reported adverse effects compared to 50 mg or 100 mg once a day [26]. In our mouse model, the mouse dose of 20 mg/kg of DIA is equivalent to 1.6 mg/kg human dose (human diacerein recommended dose) based on a conversion factor of mouse dose to human dose [47]. Besides, we found that even 40 mg/kg of DIA in mice was below the equivalent DIA human dose. Regarding the toxicity of DIA, LD_{50} of >5000 mg/kg in mice is equivalent to a DIA human dose of >6476 mg/kg (https://pubchem.ncbi.nlm.nih.gov/compound/Diacerein#section=Toxicity). The dose of DIA was 50 mg/kg where no adverse effect or no effect concentration of DIA was observed (https://www.accessdata.fda.gov/, application number: 761037Orig1s000) from the 6-month. We showed 20 mg/kg or 40 mg/kg of DIA could enhance the uptake of ^{131}I-RTX. When we compare dose-dependency between 20 mg/kg and 40 mg/kg of DIA during ^{131}I-RTX therapy, there were no significant differences between groups (shown in **Figures 3**, **4**). Therefore, 20 mg/kg of DIA during ^{131}I-RTX therapy could be used as a combination therapy drug. Graphical abstract of our combination scheme is shown in Supplementary Figure 3.

In summary, we first demonstrated that DIA was a good candidate for a combination drug for ^{131}I-RTX. RIT in combination with a DIA could synergize the therapeutic efficacy. Overall, our suggested therapeutic strategy for Burkitt's lymphoma would be a promising tool for targeted therapy in clinics.

Conclusion

We demonstrated that DIA-induced apoptosis and related this to IL-1β downstream signaling through Western blotting. Our suggested combination of DIA and ^{131}I-RTX strategies could enhance the efficacy of ^{131}I-RTX as a treatment for Burkitt's lymphoma.

Acknowledgements

This study was funded by the Ministry of Science and ICT (MSIT) (NRF-2020R1F1-A1061476, NRF-2021M2E8A1039980, 504-61-2020, 50536-2020) and supported by the Ministry of Health and Welfare (No. HO-15C0001).

Disclosure of conflict of interest

None.

Address correspondence to: Dr. Jae Jun Lee, Laboratory Animal Center, Osong Medical Innovation Foundation, Osong saengmyongro 123, Osong-eup, Cheongju-si, Chungbuk 28160, Republic of Korea. Tel: +82-43-200-9850; Fax: +82-43-200-9805; E-mail: jlee@kbiohealth.kr; Dr. Jin Su Kim, Division of RI Application, Korea Institute of Radiological and Medical Sciences, 75 Nowon-Gil, Gongneung-Dong, Nowon-Gu, Seoul 01812, Republic of Korea. Tel: +82-2-970-1661; Fax: +82-2-970-2416; E-mail: kjs@kirams.re.kr

References

[1] Hernandez MC and Knox SJ. Radiobiology of radioimmunotherapy: targeting CD20 B-cell antigen in non-Hodgkin's lymphoma. Int J Radiat Oncol Biol Phys 2004; 59: 1274-1287.

[2] Boye J, Elter T and Engert A. An overview of the current clinical use of the anti-CD20 monoclonal antibody rituximab. Ann Oncol 2003; 14: 520-535.

[3] Plosker GL and Figgitt DP. Rituximab: a review of its use in non-Hodgkin's lymphoma and chronic lymphocytic leukaemia. Drugs 2003; 63: 803-843.

[4] Larson SM, Carrasquillo JA, Cheung NK and Press OW. Radioimmunotherapy of human tumours. Nat Rev Cancer 2015; 15: 347-60.

[5] Zaheer J, Kim H, Lee YJ, Kim JS and Lim SM. Combination radioimmunotherapy strategies for solid tumors. Int J Mol Sci 2019; 20: 5579.

[6] Kim JS. Combination radioimmunotherapy approaches and quantification of immuno-PET. Nucl Med Mol Imaging 2016; 50: 104-111.

[7] Heldin CH, Rubin K, Pietras K and Ostman A. High interstitial fluid pressure-an obstacle in cancer therapy. Nat Rev Cancer 2004; 4: 806-813.

[8] Kim HG, Yu AR, Lee JJ, Lee YJ, Lim SM and Kim JS. Measurement of tumor pressure and strat-

egies of imaging tumor pressure for radioimmunotherapy. Nucl Med Mol Imaging 2019; 53: 235-241.
[9] Karttunen T, Apaja-Sarkkinen M, Alavaikko M, Blanco G, Aine R, Jarvinen M and Autio-Harmainen H. Characterization of extracellular matrix in non-Hodgkin's lymphomas. Pathol Res Pract 1988; 183: 735-746.
[10] Kim EH, Ko HY, Yu AR, Kim H, Zaheer J, Kang HJ, Lim YC, Cho KD, Joo HY, Kang MK, Lee JJ, Lee SS, Kang HJ, Lim SM and Kim JS. Inhibition of HIF-1alpha by atorvastatin during (131) I-RTX therapy in Burkitt's lymphoma model. Cancers (Basel) 2020; 12: 1203.
[11] Almezgagi M, Zhang Y, Hezam K, Shamsan E, Gamah M, Al-Shaebi F, Abbas AB, Shoaib M, Saif B, Han Y, Jia R and Zhang W. Diacerein: recent insight into pharmacological activities and molecular pathways. Biomed Pharmacother 2020; 131: 110594.
[12] Abd-Ellatif RN, Hegab, II, Atef MM, Sadek MT and Hafez YM. Diacerein protects against glycerol-induced acute kidney injury: Modulating oxidative stress, inflammation, apoptosis and necroptosis. Chem Biol Interact 2019; 306: 47-53.
[13] Mohan GC, Zhang H, Bao L, Many B and Chan LS. Diacerein inhibits the pro-atherogenic & pro-inflammatory effects of IL-1 on human keratinocytes & endothelial cells. PLoS One 2017; 12: e0173981.
[14] Davis AP, Grondin CJ, Johnson RJ, Sciaky D, McMorran R, Wiegers J, Wiegers TC and Mattingly CJ. The comparative toxicogenomics database: update 2019. Nucleic Acids Res 2019; 47: D948-D954.
[15] Pathan M, Keerthikumar S, Chisanga D, Alessandro R, Ang CS, Askenase P, Batagov AO, Benito-Martin A, Camussi G, Clayton A, Collino F, Di Vizio D, Falcon-Perez JM, Fonseca P, Fonseka P, Fontana S, Gho YS, Hendrix A, Hoen EN, Iraci N, Kastaniegaard K, Kislinger T, Kowal J, Kurochkin IV, Leonardi T, Liang Y, Llorente A, Lunavat TR, Maji S, Monteleone F, Øverbye A, Panaretakis T, Patel T, Peinado H, Pluchino S, Principe S, Ronquist G, Royo F, Sahoo S, Spinelli C, Stensballe A, Théry C, van Herwijnen MJC, Wauben M, Welton JL, Zhao K and Mathivanan S. A novel community driven software for functional enrichment analysis of extracellular vesicles data. J Extracell Vesicles 2017; 6: 1321455.
[16] Wang Z, Clark NR and Ma'ayan A. Drug-induced adverse events prediction with the LINCS L1000 data. Bioinformatics (Oxford, England) 2016; 32: 2338-2345.
[17] Mi Y, Shi Y, Li J, Liu W and Yan M. Fuzzy-based concept learning method: exploiting data with fuzzy conceptual clustering. IEEE Trans Cybern 2020; [Epub ahead of print].
[18] Lee YS, Kim HJ and Kim JS. Improved quantification of (18)F-FDG PET during (131)I-Rituximab therapy on mouse lymphoma model after (131)I prompt emission correction. Diagnostics (Basel) 2019; 9: 144.
[19] Pavelka K, Bruyere O, Cooper C, Kanis JA, Leeb BF, Maheu E, Martel-Pelletier J, Monfort J, Pelletier JP, Rizzoli R and Reginster JY. Diacerein: benefits, risks and place in the management of osteoarthritis. An opinion-based report from the ESCEO. Drugs Aging 2016; 33: 75-85.
[20] Singh K, Sharma R and Rai J. Diacerein as adjuvant to diclofenac sodium in osteoarthritis knee. Int J Rheum Dis 2012; 15: 69-77.
[21] Gadotti VM, Martins DF, Pinto HF, Oliveira G, Kaster MP, Quintao NL and Santos AR. Diacerein decreases visceral pain through inhibition of glutamatergic neurotransmission and cytokine signaling in mice. Pharmacol Biochem Behav 2012; 102: 549-554.
[22] Cardoso CRL, Leite NC, Carlos FO, Loureiro AA, Viegas BB and Salles GF. Efficacy and safety of diacerein in patients with inadequately controlled type 2 diabetes: a randomized controlled trial. Diabetes Care 2017; 40: 1356-1363.
[23] Villar MM, Martinez-Abundis E, Preciado-Marquez RO and Gonzalez-Ortiz M. Effect of diacerein as an add-on to metformin in patients with type 2 diabetes mellitus and inadequate glycemic control. Arch Endocrinol Metab 2017; 61: 188-192.
[24] Abdel-Gaber SA, Mohammed RK and Refaie MMM. Mechanism mediating the protective effect of diacerein in ischemia-reperfusion-induced testicular injury in rats. Life Sci 2018; 209: 57-62.
[25] Fouad AA, Abdel-Aziz AM and Hamouda AAH. Diacerein downregulates NLRP3/Caspase-1/IL-1beta and IL-6/STAT3 pathways of inflammation and apoptosis in a rat model of cadmium testicular toxicity. Biol Trace Elem Res 2020; 195: 499-505.
[26] Pelletier JP, Yaron M, Haraoui B, Cohen P, Nahir MA, Choquette D, Wigler I, Rosner IA and Beaulieu AD. Efficacy and safety of diacerein in osteoarthritis of the knee: a double-blind, placebo-controlled trial. The Diacerein Study Group. Arthritis Rheum 2000; 43: 2339-2348.
[27] Refaie MMM and El-Hussieny M. The role of interleukin-1b and its antagonist (diacerein) in estradiol benzoate-induced endometrial hyperplasia and atypia in female rats. Fundam Clin Pharmacol 2017; 31: 438-446.
[28] Colotta F, Allavena P, Sica A, Garlanda C and Mantovani A. Cancer-related inflammation, the

seventh hallmark of cancer: links to genetic instability. Carcinogenesis 2009; 30: 1073-1081.
[29] Guo Y, Xu F, Lu T, Duan Z and Zhang Z. Interleukin-6 signaling pathway in targeted therapy for cancer. Cancer Treat Rev 2012; 38: 904-910.
[30] Bharti R, Dey G, Banerjee I, Dey KK, Parida S, Kumar BN, Das CK, Pal I, Mukherjee M, Misra M, Pradhan AK, Emdad L, Das SK, Fisher PB and Mandal M. Somatostatin receptor targeted liposomes with diacerein inhibit IL-6 for breast cancer therapy. Cancer Lett 2017; 388: 292-302.
[31] Bharti R, Dey G, Ojha PK, Rajput S, Jaganathan SK, Sen R and Mandal M. Diacerein-mediated inhibition of IL-6/IL-6R signaling induces apoptotic effects on breast cancer. Oncogene 2016; 35: 3965-3975.
[32] Lee S, Lee HJ, Kang H, Kim EH, Lim YC, Park H, Lim SM, Lee YJ, Kim JM and Kim JS. Trastuzumab induced chemobrain, atorvastatin rescued chemobrain with enhanced anticancer effect and without hair loss-side effect. J Clin Med 2019; 8: 234.
[33] Wang S, Shin IS, Hancock H, Jang BS, Kim HS, Lee SM, Zderic V, Frenkel V, Pastan I, Paik CH and Dreher MR. Pulsed high intensity focused ultrasound increases penetration and therapeutic efficacy of monoclonal antibodies in murine xenograft tumors. J Control Release 2012; 162: 218-224.
[34] Jung BK, Ko HY, Kang H, Hong J, Ahn HM, Na Y, Kim H, Kim JS and Yun CO. Relaxin-expressing oncolytic adenovirus induces remodeling of physical and immunological aspects of cold tumor to potentiate PD-1 blockade. J Immunother Cancer 2020; 8: e000763.
[35] Holzwarth U, Ojea Jimenez I and Calzolai L. A random walk approach to estimate the confinement of alpha-particle emitters in nanoparticles for targeted radionuclide therapy. EJNMMI Radiopharm Chem 2018; 3: 9.
[36] Lassmann M and Eberlein U. Targeted alpha-particle therapy: imaging, dosimetry, and radiation protection. Ann ICRP 2018; 47: 187-195.
[37] Kozempel J, Mokhodoeva O and Vlk M. Progress in targeted alpha-particle therapy. What we learned about recoils release from in vivo generators. Molecules 2018; 23: 581.
[38] Pruszynski M, D'Huyvetter M, Bruchertseifer F, Morgenstern A and Lahoutte T. Evaluation of an Anti-HER2 nanobody labeled with (225)Ac for targeted alpha-particle therapy of cancer. Mol Pharm 2018; 15: 1457-1466.
[39] Palm S, Back T, Lindegren S, Hultborn R, Jacobsson L and Albertsson P. Model of intraperitoneal targeted alpha-particle therapy shows that posttherapy cold-antibody boost enhances microtumor radiation dose and treatable tumor sizes. J Nucl Med 2018; 59: 646-651.
[40] Milenic DE, Baidoo KE, Kim YS, Barkley R and Brechbiel MW. Comparative studies on the therapeutic benefit of targeted alpha-particle radiation therapy for the treatment of disseminated intraperitoneal disease. Dalton Trans 2017; 46: 14591-14601.
[41] Milenic DE, Baidoo KE, Kim YS, Barkley R and Brechbiel MW. Targeted alpha-particle radiation therapy of HER1-positive disseminated intraperitoneal disease: an investigation of the human anti-EGFR monoclonal antibody, panitumumab. Transl Oncol 2017; 10: 535-545.
[42] Sattiraju A, Solingapuram Sai KK, Xuan A, Pandya DN, Almaguel FG, Wadas TJ, Herpai DM, Debinski W and Mintz A. IL13RA2 targeted alpha particle therapy against glioblastomas. Oncotarget 2017; 8: 42997-43007.
[43] Yong K and Brechbiel M. Application of (212) Pb for targeted alpha-particle therapy (TAT): pre-clinical and mechanistic understanding through to clinical translation. AIMS Med Sci 2015; 2: 228-245.
[44] Al Darwish R, Staudacher AH, Li Y, Brown MP and Bezak E. Development of a transmission alpha particle dosimetry technique using A549 cells and a Ra-223 source for targeted alpha therapy. Med Phys 2016; 43: 6145.
[45] Kiess AP, Minn I, Vaidyanathan G, Hobbs RF, Josefsson A, Shen C, Brummet M, Chen Y, Choi J, Koumarianou E, Baidoo K, Brechbiel MW, Mease RC, Sgouros G, Zalutsky MR and Pomper MG. (2S)-2-(3-(1-Carboxy-5-(4-211At-Astatobenzamido)Pentyl)Ureido)-pentanedioic acid for PSMA-targeted alpha-particle radiopharmaceutical therapy. J Nucl Med 2016; 57: 1569-1575.
[46] Refaie MM, Amin EF, El-Tahawy NF and Abdelrahman AM. Possible protective effect of diacerein on doxorubicin-induced nephrotoxicity in rats. J Toxicol 2016; 2016: 9507563.
[47] Nair AB and Jacob S. A simple practice guide for dose conversion between animals and humans. J Basic Clin Pharm 2016; 7: 27-31.

Supplementary information

^{131}I-radiolabeling with RTX

^{131}I-radiolabeling with RTX was conducted as described previously [18]. After labeling, instant thin-layer chromatography (solvent, 100% C_3H_6O) showed that the radiochemical purity of ^{131}I-RTX was >95%. The immunoreactivity of ^{131}I-RTX was 95.0%, as determined using a cell-binding assay, and the specific activity was 0.32 mCi/mg (Supplementary Figure 1).

Cell viability

H460 and H1299 cells were maintained in Roswell Park Memorial Institute, and A459 and JIMT were cultured in Dulbecco's Modified Eagle Medium containing 10% fetal bovine serum with 5% antibiotics (Sigma, St. Louis, MO, USA) at 37°C in a humidified 5% CO_2 incubator. Cell viability was checked with fluorescent spectrophotometer at endpoint with wavelength 560 to 590 lambda.

DIA also induced cytotoxicity to NCI-H460, NCI-H1299, JIMT-1, and A459. Cytotoxic effect of DIA is observed in breast and lung cancer and in combination with trastuzumab by alamarBlue assay (Supplementary Figure 2).

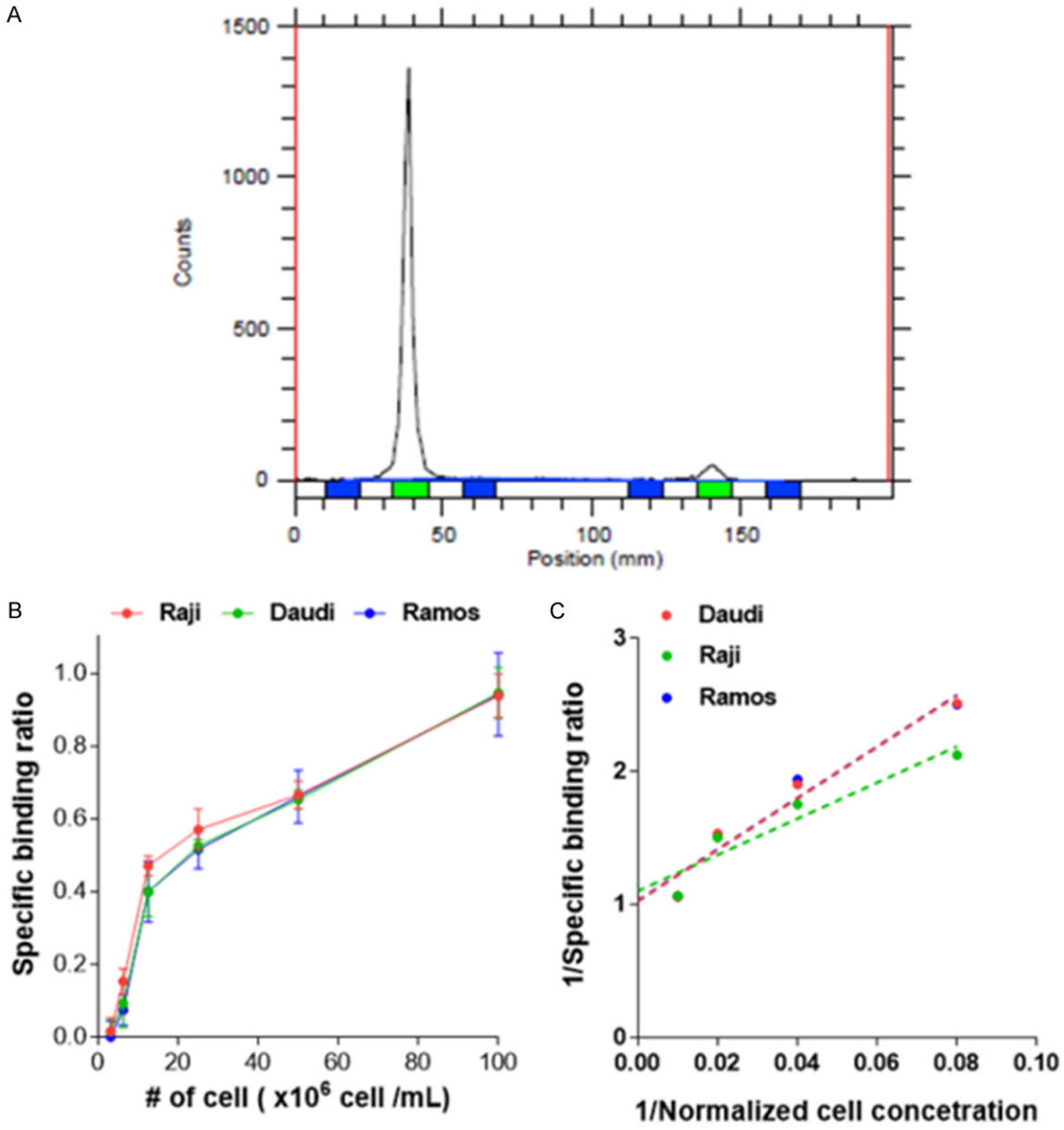

Supplementary Figure 1. ^{131}I-radiolabeling with RTX. A. After labeling, instant thin-layer chromatography (solvent, 100% C_3H_6O) showed that the radiochemical purity of ^{131}I-RTX was >95%. B, C. The immunoreactivity of 131I-RTX was 95.0%, as determined using a cell-binding assay.

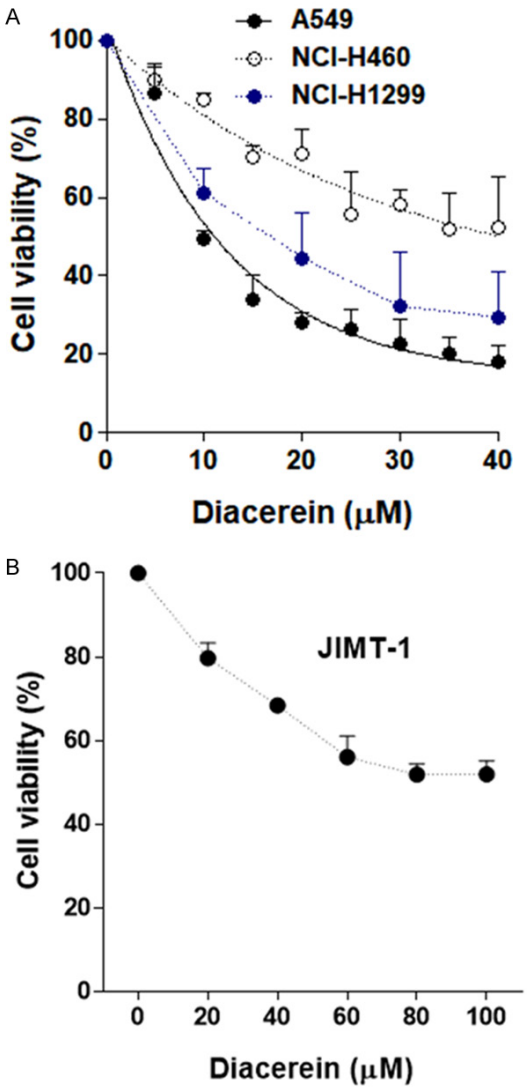

Supplementary Figure 2. Cytotoxicity. A. DIA shows cell cytotoxicity in lung cancer cell line such as A549, H460, and H1299. B. DIA also showed cytotoxicity in breast cancer cell line that is JIMT.

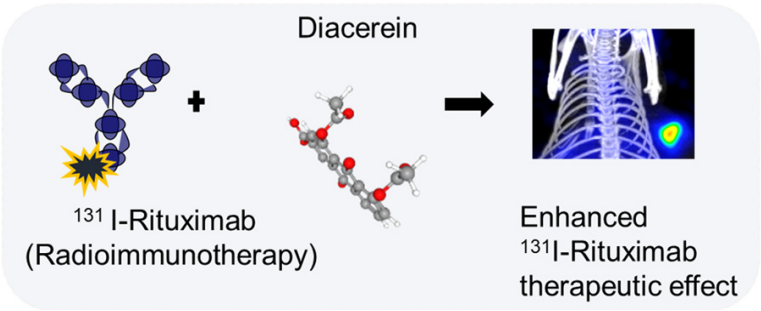

Supplementary Figure 3. Graphical abstract. Combination radioimmunotherapy (RIT) of ^{131}Iodine-Rituximab with diacerin improves RIT uptake in Burkitt's lymphoma.

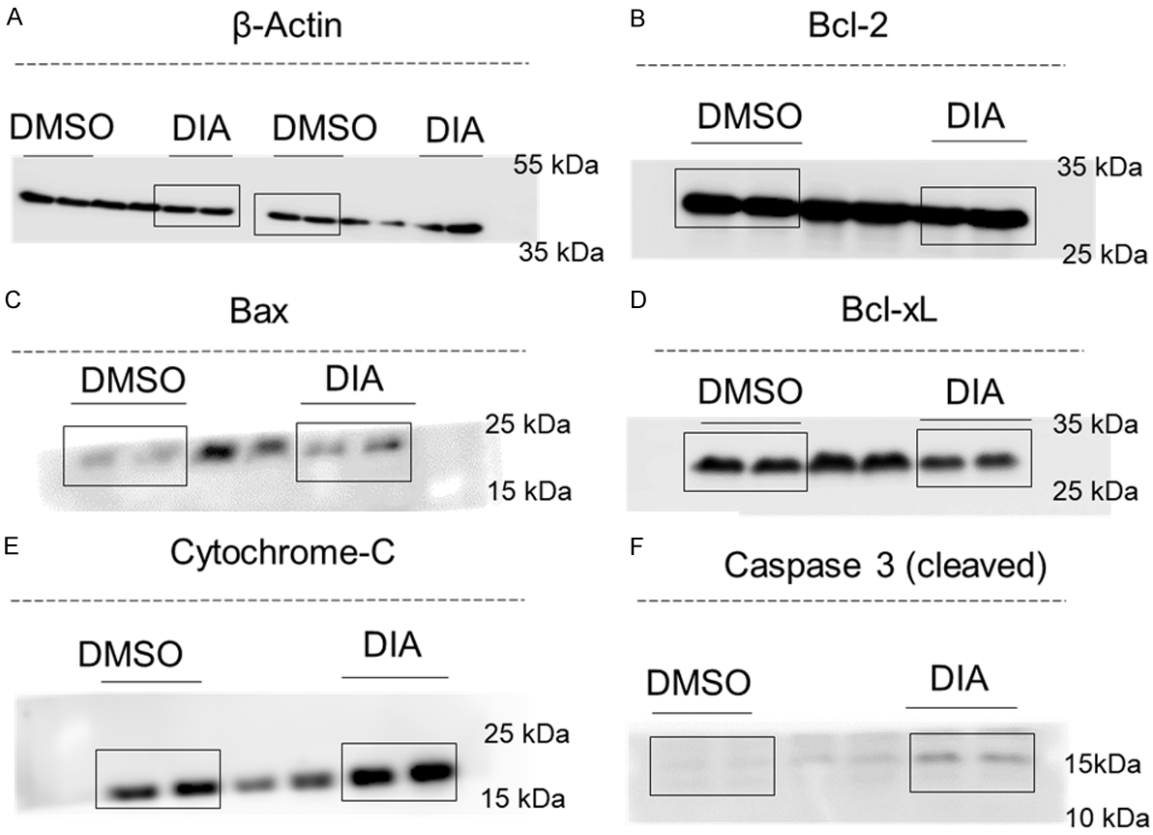

Supplementary Figure 4. Western blot full layer gels. A-F. The western blot layered gel shows selected bands (black rectangle) for DMSO and DIA treated samples for beta-Actin, Bcl-2, Bax, Bcl-xL, cytochrome-C and Caspase-3.